Homogeneous linewidth broadening and exciton dephasing mechanism in $MoTe_2$

Sandhaya Koirala,* Shinichiro Mouri, Yuhei Miyauchi, and Kazunari Matsuda†
Institute of Advanced Energy, Kyoto University, Uji, Kyoto 611-0011, Japan
(Received 5 October 2015; revised manuscript received 14 December 2015; published 4 February 2016)

Spectroscopic studies of mechanically exfoliated monolayer $MoTe_2$ were performed over a wide temperature range from 4.2 to 300 K. At a low temperature, the photoluminescence spectra for monolayer $MoTe_2$ showed two sharp peaks for excitons and charged excitons (trions). The homogeneous linewidth of the exciton peak broadened linearly as the temperature increased. This linear linewidth broadening was caused by acoustic-phonon scattering of the exciton, i.e., shortening of exciton dephasing. The broadening factor due to exciton–acoustic–phonon interactions was found to be 0.11 meV K^{-1}. This small value for the exciton–phonon coupling coefficient and the lack of a Stokes shift suggest that exciton–phonon interactions in monolayer $MoTe_2$ are in the weak coupling regime.

DOI: 10.1103/PhysRevB.93.075411

Recently, atomically thin layered transition-metal dichalcogenides (TMDs) in the form MX_2(M = Mo, W; X = S, Se, Te) have attracted much interest from the viewpoints of their fundamental physics and potential applications [1,2]. The characteristic optical features of semiconducting two-dimensional (2D) TMDs arise from bound electron-hole pairs (excitons) confined in their atomically thin layers, which play important roles in optoelectronic device applications [3,4]. Optical studies of TMDs have mainly focused on the model systems MoS_2, WSe_2, and $MoSe_2$ [2,5,6]. Newly studied molybdenum ditelluride ($MoTe_2$) is also a TMD that has attracted emerging research interest because of its novel optical properties, including optical gap energy (lowest exciton transition) of 1.09 eV, which is in the near-infrared region [7,8]. Compared with other Mo-based TMD semiconductors (MoS_2 and $MoSe_2$), $MoTe_2$ also has a stronger spin-orbit coupling of 250 meV [7], which may result in a longer decoherence time for valley and spin degree of freedoms [9,10] and therefore enable its use in valleytronic devices.

The energy and phase relaxation of excitons influenced by phonon scattering processes is an important issue in the study of low-dimensional semiconductor physics [11,12]. Indeed, the energy relaxation of excitons in TMDs has been studied by transient absorption and photoluminescence (PL) spectroscopy [13]. However, the mechanism of exciton phase relaxation in TMDs remains unclear because it is difficult to obtain information on exciton dephasing time (or the intrinsic peak linewidths in optical spectra) in well-studied MX_2 TMDs (M = Mo, W; X = S, Se) [4,14,15]. These monolayer (ML) TMDs are unintentionally heavily carrier (electron or hole) doped and thus have relatively complicated optical spectra with overlapping exciton and charged exciton (trion) spectral peaks [16]. In contrast, $MoTe_2$ is a relatively low-carrier-density semiconductor [16], which enables the precise determination of its optical spectrum and evaluation of the optical spectral linewidths for excitons.

Herein, we describe the results of spectroscopic analyses of mechanically exfoliated ML $MoTe_2$ from cryogenic temperature 4.2 K to room temperature performed in order to study exciton dephasing and exciton–phonon interactions. At low temperatures, the PL spectra for ML $MoTe_2$ exhibited two sharp excitons (X) and charged exciton (trion X^-) peaks. The homogeneous linewidth of the exciton peak increased linearly with increasing temperature, suggesting that the exciton dephasing causing the linewidth broadening was dominated by the scattering of excitons by low-energy acoustic phonons. Notably, the obtained linewidth broadening coefficient indicated that the exciton acoustic–phonon interactions in ML $MoTe_2$ are in the weak-coupling regime, which is favorable for applications requiring long exciton coherence times.

$MoTe_2$ crystals were mechanically exfoliated onto SiO_2/Si and quartz substrates in order to obtain ML flakes of $MoTe_2$. An SiO_2/Si substrate with an SiO_2 thickness of 290 nm was used to clearly identify the atomically thin materials. Atomic force microscopy (AFM) and Raman scattering analyses were conducted to identify the layer thicknesses of the exfoliated $MoTe_2$ flakes on the substrates. Raman measurements at room temperature were conducted using a micro-Raman spectrometer, RAMANtouch (532 nm, 2.33 eV) with a 100× objective (Numerical Aperture [NA] = 0.8); the signals were detected in reflection geometry. The PL and differential reflectivity measurements from 4.2 to 300 K were conducted using a home-built setup with a 100× objective (NA = 0.5), and the signals were detected using a liquid N_2-cooled InGaAs array. An excitation wavelength of ∼550 nm (2.25 eV) with a delivered power of ∼10 μW from a supercontinuum laser source was used for PL measurements. The white light with very low power ∼2 μW from the supercontinuum laser source was used for differential reflectivity measurements.

Figure 1 shows Raman scattering spectra for $MoTe_2$ consisting of different numbers of layers on SiO_2/Si substrates. The optical images of ML and bilayer (BL) $MoTe_2$ are also shown in the inset on the left side of Fig. 1. The characteristic phonon modes for ML $MoTe_2$ are observed at ∼172 (A_g^1 mode) and ∼236 cm^{-1} (E_{2g}^1 mode) in the Raman spectra. The A_g^1 phonon mode is an in-plane vibrational mode that becomes more significant as the layer thickness increases, and the E_{2g}^1 mode is due to the stacking effect of different layers where surface effects are more significant [17]. The B_{2g}^1 mode is inactive in the bulk but is allowed for few-layer $MoTe_2$ due to the breaking of translational symmetry. As expected, for bulk $MoTe_2$, only two phonon peaks at ∼174 (A_g^1 mode) and ∼234 cm^{-1} (E_{2g}^1 mode) are observed, while all three phonon peaks are observed in trilayer and BL $MoTe_2$, and the Raman

*koirala@iae.kyoto-u.ac.jp
†matsuda@iae.kyoto-u.ac.jp

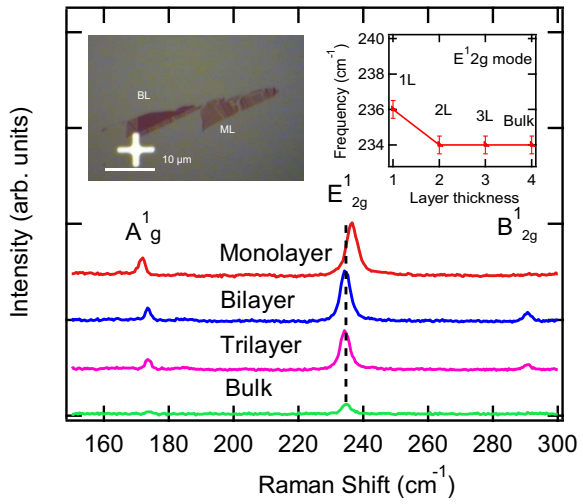

FIG. 1. Raman scattering spectra for mechanically exfoliated monolayer, bilayer, trilayer, and bulk $MoTe_2$ flakes on SiO_2/Si substrates obtained at an excitation wavelength of 532 nm. Left inset: optical microscope image of monolayer and bilayer $MoTe_2$ on SiO_2/Si substrates. Right inset: frequency shift of the E^1_{2g} mode as a function of layer thickness.

intensity increases with a decrease in the number of layers (Fig. 1). In contrast, from BL to ML $MoTe_2$, the B^1_{2g} mode disappears and characteristic up and down shifts of the A^1_g and E^1_{2g} modes, respectively, are observed in the Raman spectrum, as shown in Fig. 1. Moreover, a frequency shift of 2 cm^{-1} for the E^1_{2g} mode is observed, as shown in the inset on the right side of Fig. 1, which is significant proof of the formation of ML $MoTe_2$ and consistent with a previously reported result [7].

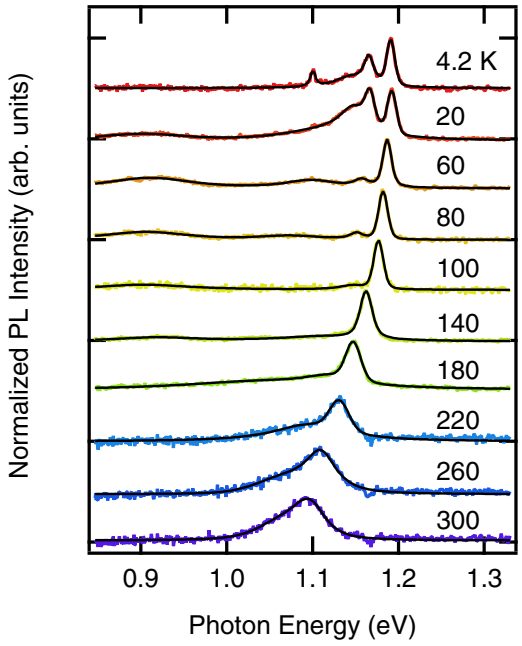

FIG. 2. Temperature dependence of the PL spectra for monolayer $MoTe_2$ and fitted results obtained using Voigt functions. The PL spectra are normalized by the intensity of the exciton peak. Each spectrum is vertically shifted for clarity.

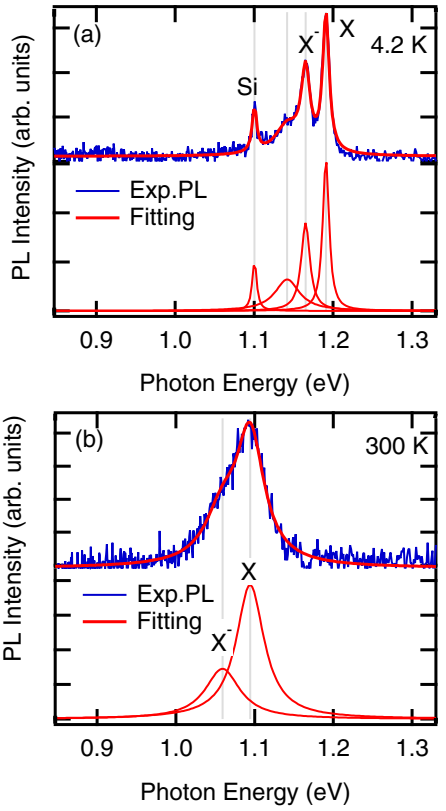

FIG. 3. PL spectra and fitted results for monolayer $MoTe_2$. (a) Upper panel: PL spectrum (blue line) and spectral fitted result obtained using the sum of Voigt functions (red line) at 4.2 K. Lower panel: each component of the spectral peak. (b) Upper panel: PL spectrum (blue line) and spectral fitted result using the sum of Voigt functions (red line) at room temperature. Lower panel: each component of the spectral peak.

The formation of ML $MoTe_2$ is also experimentally confirmed, determining the height profile of a sample using AFM.

Temperature-dependent PL spectra for ML $MoTe_2$, for which the layer number was confirmed by Raman scattering, as shown in Fig. 1, were then obtained from 4.2 to 300 K and are shown in Fig. 2. The PL spectrum at 4.2 K has two prominent peaks at 1.19 and 1.17 eV as well a peak due to the Si substrate at 1.10 eV. The two peaks are assigned as emissions from excitons (X) and charged excitons (trions X^-), respectively [8,18,19]. The energy separation between the exciton and trion peaks is approximately ~20 meV, which is lower than that in other TMD materials [14]. For ML $MoTe_2$ on a quartz substrate, only a PL peak at 1.18 eV attributed to exciton recombination is observed at 4.2 K (see the Supplemental Material, Fig. S1 [20]). The relative PL intensity of the exciton and trion peaks varied from flake to flake on the same substrate and on the two different substrates (SiO_2/Si or quartz) because the doped carrier density changes depending on the degree of charge transfer from the substrate to ML TMDs [21]. The observed PL peaks broaden and shift to lower energies with increasing temperature. The PL spectra were analyzed using spectral fitting procedures in order to evaluate the energy positions and spectral linewidths.

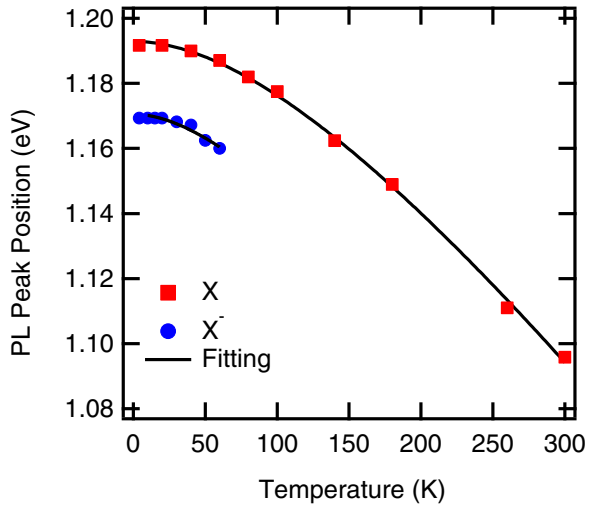

FIG. 4. Temperature dependence of the exciton (red solid squares) and trion (blue solid circles) peak positions in PL spectra for monolayer $MoTe_2$ and fitted lines obtained using the Varshni equation [Eq. (1)].

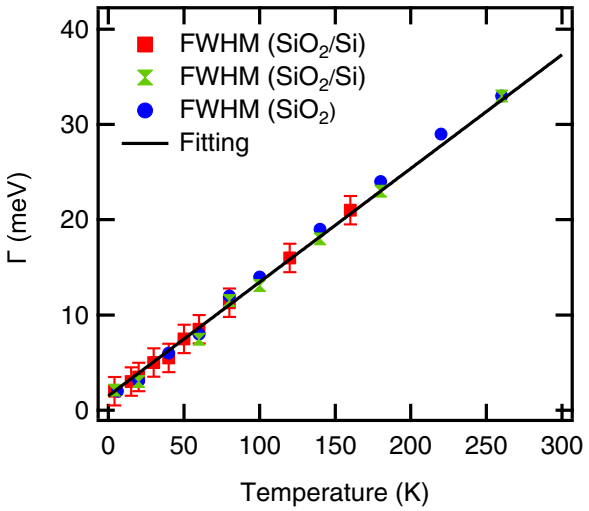

FIG. 5. The FWHM of the exciton peak linewidth in PL spectra for monolayer $MoTe_2$ plotted as a function of temperature. The solid line represent the fitted results obtained using Eq. (2). The experimental results for three different monolayer $MoTe_2$ flakes on SiO_2/Si and SiO_2 are shown in the figure.

Figures 3(a) and 3(b) show the PL spectra and fitted results (solid black lines) for ML $MoTe_2$ at low temperature 4.2 K and room temperature, respectively. The PL spectra for ML $MoTe_2$ are well reproduced using Voigt functions, which takes into account the contributions of homogeneous and inhomogeneous broadening as Lorentzian and Gaussian components, respectively (Figs. 2 and 3). Here, the two PL peaks for the excitons and charged excitons (trions) are mainly considered. Moreover, the PL spectra in the wide temperature range from 4.2 to 300 K are well fitted by these Voigt functions, as shown in Fig. 2.

Figure 4 shows the energy positions of the peaks for the excitons (solid squares) and trions (blue solid circles) as a function of temperature. Both exciton and trion peaks gradually shift to lower energies with an increase in temperature from 4.2 to 300 K. The spectral energy position of the exciton peak $E_g(0)$ is simulated using the Varshni equation [22],

$$E_{ex(tr)}(T) = E_{ex(tr)}(0) - \frac{\alpha T^2}{T+\beta}, \quad (1)$$

where T is the temperature of the ML $MoTe_2$, α and β are parameters, and $E_{ex(tr)}(0)$ is the spectral energy position of the excitons (trions) at the zero temperature limit. As shown by the solid lines in Fig. 4, the temperature dependence of the spectral shifts for both excitons and trions in ML $MoTe_2$ is well reproduced using Eq. (1). Values for $E_{ex}(0)$ of 1.19 and 1.17 eV were obtained for the exciton and trion peaks, respectively, and the values for α and β were determined to be 6.4×10^{-4} eV K^{-1} and 287 K, respectively. The Varshni equation is known to effectively describe the temperature dependence of band gap shifts in semiconductors. Therefore, the excellent reproduction of the temperature dependence of the exciton (trion) energies using the Varshni equation indicates that the energy of the exciton (trion) peak shift originated from the temperature dependent bandgap shift. It should be noted that we also confirm that the temperature dependence of the exciton (trion) energies is well reproduced using the Vinna equation (see Supplemental Material S4 [20]) [23].

As mentioned above, the PL spectra for ML $MoTe_2$ from 4.2 to 300 K were well reproduced by the fitted results obtained using Voigt functions (solid black lines in Fig. 2). The full width at half maximum (FWHM) of the Lorentzian component, which corresponds to the homogeneous linewidth, as a function of temperature for the exciton peaks for three different ML $MoTe_2$ (two on SiO_2/Si and one on SiO_2) are plotted in Fig. 5. Here, we used the fact that the FWHM of the Gaussian component corresponding to inhomogeneous broadening is 9 meV, which is independent of temperature from the analysis of lowest temperature at 4.2 K PL spectra. It can be clearly seen that the homogeneous linewidths for the exciton peaks broadens linearly with increasing temperature. Moreover, the homogeneous broadening coefficients for the three different ML flakes (two flakes on SiO_2/Si and third on SiO_2) are nearly coincident, suggesting that the obtained values for the broadening coefficient reflect the intrinsic properties of ML $MoTe_2$. Homogeneous linewidths are generally determined by exciton dephasing, which is mainly caused by exciton–phonon scattering and the radiative and nonradiative decay of excitons. Assuming a typical reported exciton relaxation time for TMDs greater than several picoseconds [24], the contribution to the linewidth from the exciton lifetime $\ll$1 meV is expected to be negligible. Thus, the homogeneous linewidth broadening Γ is attributed to exciton–phonon scattering and is described as follows [12]:

$$\Gamma = \Gamma_0 + AT + \frac{B}{\exp(\hbar\omega/k_BT)-1}, \quad (2)$$

where Γ_0 is the residual linewidth at $T = 0$ K, A and B are exciton–phonon coupling constants for the low- and high-frequency phonon modes, respectively, $\hbar\omega$ is the energy of the high-frequency phonon mode, and k_B is Boltzmann's constant. The solid line in Fig. 5 shows the fitted result obtained

using Eq. (2), and it can be clearly seen that they are in good agreement with the homogeneous linewidth broadening observed experimentally. The temperature dependence of the homogeneous linewidth exhibits nearly linear behavior over the wide temperature range from 4.2 to 300 K, suggesting that the contributions of the high-frequency optical phonons are negligible and that exciton scattering with low-frequency acoustic phonons is the main cause of the homogeneous broadening of the exciton peak in the PL spectra for ML $MoTe_2$.

The value of the exciton–phonon coupling constant A was determined to be 0.11 meV K^{-1} for ML $MoTe_2$ on an SiO_2/Si substrate. Note that the same value was also obtained for ML $MoTe_2$ on a quartz substrate (see Supplemental Material, Fig. S4 [20]). This value of A (0.11 meV K^{-1}) reflects the strength of exciton–phonon coupling and is nearly on the same order as the reported values for III-V (GaAs/AlGaAs) and II-VI (CdSe/ZnSe) semiconductor quantum wells [25,26]. The small values for A (0.11 meV K^{-1}) and $B \sim (0)$ meV K^{-1} suggest that ML $MoTe_2$ exists in the relatively weak exciton–phonon coupling regime. The energy difference between exciton absorptions and PL peaks, namely the Stokes shift, is another measure of exciton–phonon coupling and can be used to confirm the strength of exciton–phonon interactions [27]. Thus, we measured the differential reflectivity spectra for ML $MoTe_2$ on a transparent quartz substrate (see Supplemental Material, Fig. S1 [20]), which are close approximation of the absorption spectra [7]. Note that the exciton peaks in the differential reflectivity and PL spectra appear at the same energies, indicating a very small Stokes shift of less than 1 meV (see Supplemental Material, Fig. S2 [20]). The very small Stokes shift also suggests that the exciton–phonon interactions in ML $MoTe_2$ are in the weak coupling regime, which is favorable for applications that require longer exciton coherence times [28].

In summary, we studied the PL and differential reflectance spectra for mechanically exfoliated ML $MoTe_2$ from 4.2 to 300 K. The PL spectra for ML $MoTe_2$ showed two sharp exciton and charged exciton (trion) peaks at low temperature. The homogeneous linewidth of the exciton peak showed linear linewidth broadening with increasing temperature. The linear behavior of this temperature-dependent homogeneous linewidth broadening was attributed to acoustic-phonon scattering of excitons, which resulted in shortening of the exciton dephasing time. The homogeneous broadening factor due to these exciton–acoustic–phonon interactions was determined to be 0.11 meV K^{-1}. This relatively small value for the exciton–phonon coupling coefficient and the lack of a Stokes shift suggest that the exciton–phonon interactions in ML $MoTe_2$ are in the weak-coupling regime. Consequently, ML $MoTe_2$ as an atomically thin-layered TMD has significant potential for use in optoelectronic device applications.

The authors acknowledge S. Konabe for his fruitful discussions. This paper was supported by Grants-in-Aid for JSPS KAKENHI (Grants No. 22740195, No. 25400324, No. 25246010, No. 15K135001, No. 26107522, No. 23340085, and No. 25610074) and by Precursory Research for Embryonic Science and Technology (PRESTO) from the Japan Science and Technology Agency (JST).

[1] B. Baugher, H. Churchill, Y. Yang, and P. Jarillo-Herrero, Nat. Nanotech. **9**, 262 (2014).
[2] Q. Wang, K. Kalantar-Zadeh, A. Kis, J. N. Coleman, and M. S. Strano, Nat. Nanotech **7**, 699 (2012).
[3] K. Fai Mak, K. He, C. Lee, G. H. Lee, J. Hone, T. F. Heinz, and J. Shan, Nat. Mater. **12**, 207 (2013).
[4] Y. Lin, X. Ling, L. Yu, S. Huang, A. L. Hsu, Y-H. Lee, J. Kong, M. S. Dresselhaus, and T. Palacios, Nano Lett. **14**, 5569 (2014).
[5] G. Wang, L. Bouet, D. Lagarde, M. Vidal, A. Balocchi, T. Amand, X. Marie, and B. Urbaszek, Phys. Rev. B **90**, 075413 (2014).
[6] N. Zibouche, P. Philipsen, A. Kuc, and T. Heine, Phys. Rev. B **90**, 125440 (2014).
[7] C. Ruppert, O. B. Aslan, and T. F. Heinz, Nano Lett. **14**, 6231 (2014).
[8] I. G. Lezama, A. Arora, A. Ubaldini, C. Barreteau, E. Giannini, M. Potemski, and A. F. Morpurgo, Nano Lett. **15**, 2336 (2015).
[9] N. R. Pradhan, D. Rhodes, S. Feng, Y. Xin, S. Memaran, B.-H. Moon, H. Terrones, M. Terrones, and L. Balicas, ACS Nano **8**, 5911 (2014).
[10] H. Guo, T. Yang, M. Yamamoto, L. Zhou, R. Ishikawa, K. Ueno, K. Tsukagoshi, Z. Zhang, M. S. Dresselhaus, and R. Saito, Phys. Rev. B **91**, 205415 (2015).
[11] H. Zhao, S. Wachter, and H. Kalt, Phys. Rev. B **66**, 085337 (2002).
[12] D. Karaiskaj and A. Mascarenhas, Phys. Rev. B **75**, 115426 (2007).
[13] A. V. Trifonov, S. N. Korotan, A. S. Kurdyubov, I. Y. Gerlovin, I. V. Ignatiev, Yu P. Efimov, S. A. Eliseev, V. V. Petrov, Yu. K. Dolgikh, V. V. Ovsyankin, and A. V. Kavokin, Phys. Rev. B **91**, 115307 (2015).
[14] M. Yamamoto, S. T. Wang, M. Ni, Y.-F. Lin, S.-L. Li, S. Aikawa, W.-B. Jian, K. Ueno, K. Wakabayashi, and K. Tsukagoshi, ACS Nano **8**, 3895 (2014).
[15] C. Mai, A. Barrette, Y. Yu, Y. G. Semenov, K. W. Kim, L. Cao, and K. Gundogdu, Nano Lett. **14**, 202 (2014).
[16] S. Fathipour, N. Ma, W. S. Hwang, V. Protasenko, S. Vishwanath, H. G. Xing, H. Xu, D. Jena, J. Appenzeller, and A. Seabaugh, Appl. Phys. Lett. **105**, 192101 (2014).
[17] T. J. Wieting, A. Grisel, and F. Levy, Physica B & C **99**, 337 (1980).
[18] M. Z. Bellus, F. Ceballos, H.-Y. Chiu, and H. Zhao, ACS Nano **9**, 6459 (2015).
[19] J. Yang, T. Lu, Y. W. Myint, J. Pei, D. Macdonald, J.-C. Zheng, and Y. Lu, ACS Nano **9**, 6603 (2015).
[20] See Supplemental Material at http://link.aps.org/supplemental/10.1103/PhysRevB.93.075411 which includes the details of PL and differential reflectance measurements on quartz substrate.
[21] Y. Li, Z. Qi, M. Liu, Y. Wang, X. Cheng, G. Zhang, and L. Sheng, Nanoscale **6**, 15248 (2014).

[22] N. M. Ravindra and V. K. Srivastava, J. Phys. Chem. Solids **40**, 791 (1979).

[23] L. Vinna, S. Logothetidis, and M. Cardona, Phys. Rev. B **30**, 1979 (1984).

[24] Q. Cui, F. Ceballos, N. Kumar, and H. Zhao, ACS Nano **8**, 2970 (2014).

[25] J. Feldmann, G. Peter, E. O. Gobel, P. Dawson, K. Moore, C. Foxon, and R. J. Elliott, Phys. Rev. Lett. **59**, 2337 (1987).

[26] D. S. Citrin, Solid State Commun. **84**, 281 (1992).

[27] S. Koirala, M. Takahata, Y. Hazama, N. Naka, and K. Tanaka, J. Lumi. **155**, 65 (2014).

[28] G. Moody, C. K. Dass, K. Hao, C.-H. Chen, L.-J. Li, A. Singh, K. Tran, G. Clark, X. Xu, G. Bergäuser, E. Malic, A. Knorr, and X. Li, Nat. Commun. **6**, 8315 (2015).